scientific reports

Check for updates

OPEN

Targeted delivery of doxorubicin to B-cell lymphoma using monoclonal antibody-functionalized Chaetoceros biosilica

Ghazal Salari[1], Ahmad Shadi[1]✉, Amirhossein Ahmadi[1], Javid Esfandyari[2] & Hossein Nikmanesh[3]

The use of biogenic nanoparticles as targeted drug delivery systems has gained increasing attention for improving anticancer therapies. This study investigates the effectiveness of porous biosilica derived from the diatom *Chaetoceros* sp., functionalized with hydrophilic GPTMS, labeled with CD-19 antibody, and loaded with doxorubicin in targeting Raji cells, a B lymphoid cell line. Biosilica was extracted, purified, and modified for enhanced drug delivery. Characterization involved X-ray diffraction (XRD), Brunauer–Emmett–Teller (BET) analysis, zeta potential measurement, dynamic light scattering (DLS), Transmission Electron Microscopy (TEM), scanning electron microscopy (SEM), and Fourier-transform infrared (FT-IR) spectroscopy, followed by drug loading and release measurements. Cytotoxicity was assessed using the MTT assay and apoptosis tests, with Jurkat cells as non-target controls. Results confirmed successful GPTMS surface modification and revealed the amorphous structure of biosilica, with mean intraparticle pore sizes of 130 nm (BET). The drug loading capacity reached 53.92%. The system exhibited significant cytotoxic effects on Raji cells (IC₅₀ = 0.1 mg/mL), with lower Jurkat cell survival ($p < 0.05$). Enhanced apoptosis was detected in Raji cells. These findings suggest the modified biosilica has substantial potential for targeted drug delivery, with the antibody enhancing attachment and release at target sites. Further investigation is needed to address biocompatibility and bioaccumulation for in vivo applications.

Keywords Targeted drug delivery, Doxorubicin, Diatom, B-cell Lymphoma, CD19

Lymphomas, a group of heterogeneous malignancies, are among the leading causes of cancer-related mortality worldwide[1]. Lymphomas account for approximately 5% of malignancies with an estimated survival rate of 72%[2].

They arise from the clonal proliferation of B-cell, T-cell, and natural killer (NK) cells. Lymphomas are generally categorized into two main types: Hodgkin's lymphoma (HL) and non-Hodgkin's lymphoma (NHL). The incidence of NHL surpasses that of HL by approximately sevenfold, positioning it as the eighth most prevalent cancer worldwide[3]. NHL is more prevalent among men than women and accounts for approximately 4% of all cancer diagnoses and annual mortality[4].

Non-Hodgkin's lymphoma (NHL) is a heterogeneous class of cancers that arise in lymph nodes or other lymphoid tissues such as the spleen and thymus, exhibiting diverse biological phenotypes, clinical behaviors, and prognoses. According to the American Cancer Society (ACS), the incidence of NHL is increasing annually and has become one of the significant causes of cancer-related mortality due to its poor treatment response.

Lymphomas, are primarily treated through chemotherapy regimens such as cyclophosphamide, vincristine, doxorubicin, and dexamethasone[5]. However, minimizing the undesirable effects of chemotherapy remains a challenge. Doxorubicin (DOX) is an effective chemotherapeutic drug against lymphoma, however, it is accompanied by adverse effects such as dose-dependent side effects, short biological half-life, and cardiotoxicity resulting from its non-specific biological distribution[2,4].

One of the main problems in the treatment of B-cell lymphoma is the severe side effects and low therapeutic efficacy resulting from systemic chemotherapy. Although these treatments are often associated with desirable

[1]Department of Biological Science and Technology, Persian Gulf University, Bushehr 751691, Iran. [2]The Persian Gulf Marine Biotechnology Research Center, The Persian Gulf Biomedical Sciences Research Institute, Bushehr University of Medical Sciences, Bushehr, Iran. [3]Department of Physics, Persian Gulf University, Bushehr, Iran. ✉email: shadi@pgu.ac.ir

therapeutic effects, significant undesirable effects may occur due to early drug release before reaching the intended sites and non-specific biodistribution in normal tissues[2,4]. These limitations serve to constrain the successful clinical application of such a chemotherapy regimen. Therefore, investigating new therapeutic strategies to prevent premature drug release in the bloodstream, control non-specific biodistribution of drugs, reduce off-target toxicity, and improve therapeutic efficacy is essential. consequently, various biocompatible drug carriers, such as liposomes[6], metal nanoparticles[7,8], dendrimers[9], polymers[10], carbon nanomaterials[11] have been investigated for efficient targeted delivery. Porous silica nanoparticles, a promising group of such nanocarriers have garnered significant attention due to their unique properties, including large surface area, controllable particle size, good biocompatibility, and facile chemical functionalization[12–14]. Considering the laborious and costly production process of synthesized mesoporous silica NPs that also involves toxic chemicals, there has been a growing demand for more biocompatible natural alternatives. The three-dimensional nanostructured biosilica from diatom frustules is considered the most promising naturally available low-cost reservoir of mesoporous silica to develop targeted drug delivery strategies[15–17]. Diatoms are a diverse group of unicellular photosynthetic microalgae covered with porous silicified microshells known as frustule. Surface modification and functionalization have been used to improve and develop new potentials of diatom silica[18–20].

Cell targeting is a fundamental issue in the development of new strategies for the diagnosis, prediction, imaging, and treatment of specific diseases[21–24]. To achieve this goal, antibodies have been extensively used in medicine and have demonstrated promising potential. However, their production, immunogenicity, temperature sensitivity, the need for individual optimization, and high costs limit their utilization. CD19 is a 95 kDa glycoprotein belonging to the immunoglobulin superfamily and is exclusively expressed on the surface of B lymphocytes. It has recently been used as a target for therapeutic approaches[25,26]. As the main co-receptor of the B cell antigen receptor, CD19 has been shown to provide a high-affinity binding site[27].

Recent research in silica nanomedicine have improved cancer therapy strategies. Li et al.[28] introduced a dual-functional mesoporous silica that combines doxorubicin with immunostimulatory CpG oligonucleotides, enhancing efficacy through chemo-immunotherapy. Wang et al.[29] developed tumor-responsive silica nanoparticles that release drugs in acidic environments, targeting tumors effectively. However, these systems face challenges related to complex manufacturing and biocompatibility.

Our study introduces Chaetoceros-derived biosilica, which offers natural biocompatibility and hierarchical porosity. By engineering CD19 antibody-conjugated biosilica for doxorubicin delivery, we provide targeted lymphoma therapy that maintains the advantages of prior silica systems—pH-responsiveness and potential immunomodulation—while enhancing clinical applicability through sustainable production and reduced toxicity.

The present study aimed to explore the use of Chaetoceros diatom silica microshells as biocarriers for the targeted delivery of drugs to lymphoma cancer cells. To achieve a novel system for the targeted release of doxorubicin (DOX) in lymphoma, the porous frustules of Chaetoceros were modified and functionalized with 3-glycidyloxypropyl trimethoxysilane (GPTMS) and a CD19 antibody.

Materials and methods

Materials

Chaetoceros sp. was obtained from Bushehr Fisheries Research Center (Bushehr, Iran). Materials for Chaetoceros cultivation ($NaNO_3$, Na2SiO_3 0.9H_2O, NaH_2PO_4, $NaMoO_4$.2H_2O $CuSO_4$.5H_2O, $FeCl_3$.6H_2O, Na2EDTA, $ZnSO_4$.7H2O, $MnCl_2$.4H_2O, $CoCl_2$.6H_2O, Thiamine HCL, Biotin, and Vitamin B12) were purchased from the Merck. 3-glycidoxypropyl trimethoxysilane (GPTMS), ethanol, and trypan blue were provided from Sigma. Phosphate buffer saline (PBS) was obtained from DNAbiotech (Tehran, Iran).

Chaetoceros sp. cell culture

The marine diatom *Chaetoceros sp.* was rendered and cultivated axenically by inoculation in 250 mL conical flasks containing 150 ml of sterile fresh Guillard's F/2 culture medium. The diatoms were grown for 10 days in diluted seawater (25 ppt), at a constant temperature of 30 °C, under 2000 lx light intensity, and a 16:8 light: dark photoperiod regime.

Biosilica preparation

To prepare biosilica (BS) from diatom frustules, the grown biomass was isolated from the culture medium by centrifuging at 5000 rpm for 5 min then rinsed 3 times with ddH_2O. Then biomass was cleaned from organic compounds by incubating in hydrogen peroxide (H2O2) by a 30% ratio (wt. of the biomass) for 2 h at 250 °C. The samples were then treated with 250 ml of 5 M HCl for 12 h at 80 °C. Afterward, the frustules were centrifuged at 5000 rpm for 15 min, washed several times with ddH2O, and kept at 4 °C.

Surface modification of GPTMS groups onto the Biosilica

3-glycidoxypropyltrimethoxysilane (GPTMS) is a bifunctional coupling agent with high binding affinity to silica-containing epoxy groups that are reactive with amides, thiols, alcohols, and acids. Modified biosilica (MBS) was fabricated for surface functionalization of frustule-cleaned biosilica by utilizing GPTMS. 125 g of biosilica samples were suspended in 50 ml of dry toluene by stirring[30]. A total of 5 ml of GPTMS (5 M) was added gradually to the suspension was incubated for 12 h at 85 °C under constant stirring in an argon atmosphere. Afterward, the suspension was centrifuged, washed with toluene, and dried at 60 °C.

Characterization of fabricated carrying system

Surface-modified biosilica characteristics were evaluated using different methods. X-ray diffraction (XRD) patterns of the samples were measured using a D8Advance system (Bruker, Germany). Transmission electron

microscopy (TEM) analysis was performed to inspect the frustules and surface-modified biosilica using a 100 kV Philips EM208S transmission electron microscope (FEI Company, Eindhoven, The Netherlands). In addition, the microstructure and morphology of biosilica particles were visualized with a KYKY-EM3200 digital scanning electron microscope (SEM) instrument.

The FTIR spectral analysis of the synthesized carrier system was carried out on an FTIR spectrophotometer (FT/IR 4600, JASCO, Japan). Dynamic light scattering (DLS) and zeta potential analysis were performed using a Zetasizer (Zeta compact, CAD, France) to evaluate the particle size and surface charge of modified frustules. The specific surface areas and pore size distributions were obtained through the Brunauer–Emmett–Teller (BET) measurement method using the Asap2020 instrument (Micromeritics, USA).

Drug loading efficacy

In the present study, modified biosilica was examined as a model cargo for drug-carrying. Doxorubicin (DOX) was selected as a widely used chemotherapeutic agent. The standard calibration curve was constructed spectrophotometrically (m51, Bell, Italy) over the doxorubicin concentration ranges of 0.005–0.0629 and absorbance range from about 320 nm to 740 nm. To evaluate loading efficiency, 10 mg of modified porous biosilica powder was mixed with 0.2 mg/ml of doxorubicin solution at room temperature for 24 h. Thereafter, the mixture was centrifuged at 14000 rpm and unloaded DOX in the supernatant was determined using a microplate reader (Synergy H1, Biotek, USA) absorbance at 484 nm based on the constructed calibration curve. The ratio of loading was calculated via the following formula:

$$\text{Loading efficiency}(\%) = \frac{\text{Total amount of drug} - \text{Free drug in the supernant}}{\text{Total amount of drug}} \times 100$$

In vitro drug release

To prepare the antiCD19-MBS/DOX complex, 1 ml of the anti-CD19 monoclonal antibody was added to the fabricated MBS/DOX, and the suspension was stirred for 12 h at 4 °C. The resulting antiCD19-MBS/DOX was washed and maintained in PBS (pH = 7.2) for further use.

The encapsulation efficiency (EE) of the DOX-loaded Purified Chaetoceros (PC) was calculated using the following equation:

$$\text{EE} = \frac{\text{M}_0 - \text{M}_\text{s}}{\text{M}_0} \times 100\%$$

where M_0 is the total mass of DOX used for drug loading, and Ms is the mass of DOX present in the supernatant after drug loading.

The release properties of the DOX-loaded PC were tested under different pH conditions (pH 5.0 and 7.5). The loaded PC was suspended in 6 mL of phosphate buffer solution (pH 5.0 and 7.5).

Cell culture

Jurkat T-cell Leukemia ($CD19^-$) and Raji B-cell lymphoma cell lines ($CD19^+$) were purchased from the Iranian Biological Resource Center (IBRC, Tehran, Iran). The cells were cultured using RPMI 1640 culture medium (Bio-Idea, Iran) supplemented with 10% of fetal bovine serum (FBS) (Thermo Fisher Scientific), and antibiotics (100 U ml^{-1} penicillin, and 100 U ml^{-1} streptomycin) (Bio-Idea, Iran) at 37 °C in a humidified atmosphere containing 5% CO_2.

The qualitative fluorescent microscopy bioimaging of anti-CD19 MBS/DOX cellular uptake

Raji and Jurkat cells were seeded into 24-well plates at a density of 1×10^5 cells per well. The cells were then treated with anti-CD19 MBS/DOX at a concentration of 0.12 mg/mL for 4 h to facilitate cellular uptake. Following incubation, the cells were washed three times with phosphate-buffered saline (PBS) to remove any unbound anti-CD19 MBS/DOX. The intrinsic fluorescent properties of the biosilica component, which emits at approximately 520 nm when excited at 488 nm, were utilized to assess the cellular uptake of anti-CD19 MBS/DOX. After washing, the cells were resuspended in PBS, mounted onto glass slides, and imaged using a fluorescence microscope with appropriate filters for green fluorescence detection (excitation: 488 nm; emission: 520 nm).

MTT assay

The MTT kit (BioIdea, Iran) was used to study the cytotoxic effect of anti-CD19-MBS/DOX complex against Burkitt lymphoma cells. The Raji cell line was selected as the target tumor cells ($CD19^+$) in the MTT assay. Additionally, the Jurkat cell line, a $CD19^-$ cell, was used as a model to study the cytotoxic effect of anti-CD19-MBS/DOX complex against non-target cells. To perform a MTT assay, both cell lines was cultured in 96 well plates at a number of 1×10^5 cells per well. The plates were incubated at 37 °C in a humidified atmosphere containing 5% CO_2 overnight.

The Raji cells and Jurkat cells were then treated with various concentrations of anti-CD19-MBS/DOX complex (0, 0.1, 0.2, 0.4, 0.8, 1.6, 3.2 $mg.ml^{-1}$) and incubated for 24 h. Subsequently, 10 µl of MTT solution (5 $\mu g.ml^{-1}$) was added to each well and the plate was incubated at 37 °C for 4 h. Finally, 100 µl of lysis buffer from the Kit was added to each well to dissolve formazan crystals. Next, the plate was incubated for 30 min at 37 °C and the optical density (OD) of each well was measured using an automated plate reader (BioteK, UK) at the wavelength of 570 nm. The mean OD of wells treated with different concentrations of antiCD19-MBS/DOX

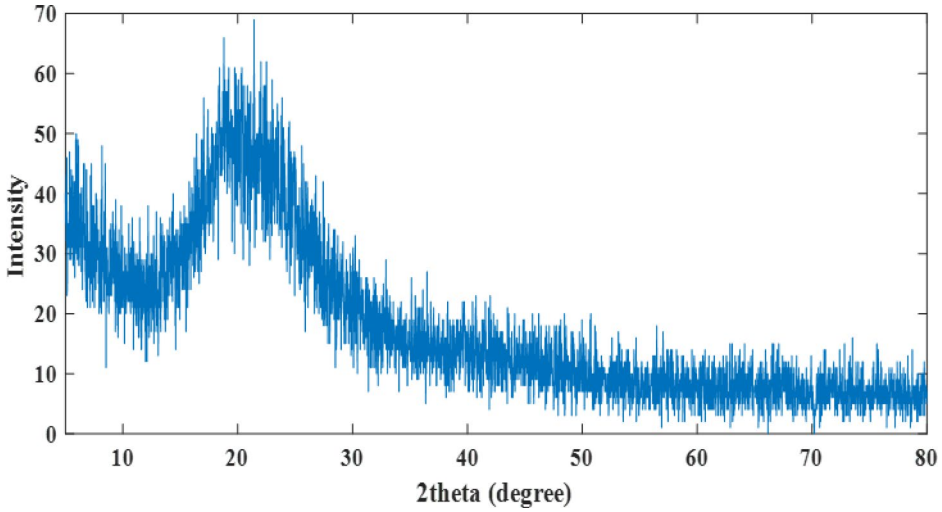

Fig. 1. XRD pattern of biosilica extracted from *Chaetoceros* sp.

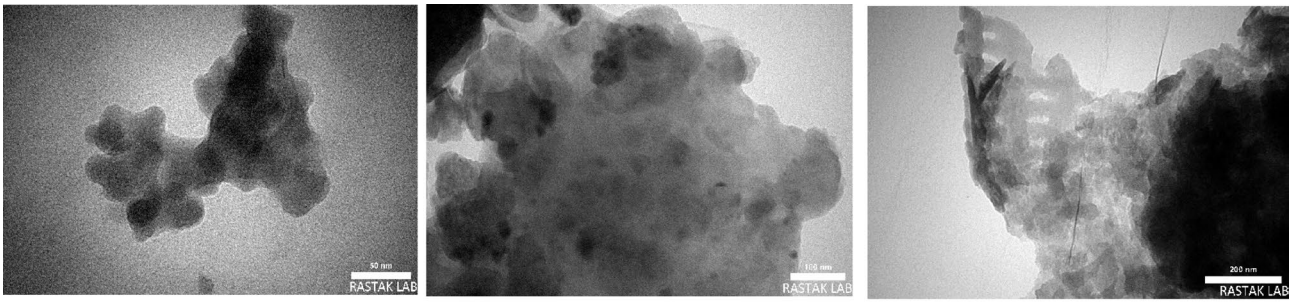

Fig. 2. Transmission electron microscopy images of biosilica extracted from *Chaetoceros* sp.

complex was divided by the mean OD of untreated wells and presented as relative OD absorbance. The tests were carried out in five replicates, and the IC_{50} value was calculated using GraphPad Prism 8.0.

Apoptosis assay by Annexin V-FITC/PI staining

To study the effects of anti-CD19-MBS/DOX complex on cell apoptosis in $CD19^+$ and $CD19^-$ cells, the Annexin V-FITC/Propidium Iodide (PI) kit (Biolegend, USA) was used according to the manufacturer's protocol. Briefly, 6×10^5 Raji or Jurkat cells were cultured in a 6-well plate and treated with an IC_{50} concentration of anti-CD19-MBS/DOX complex or left untreated. After 24 h, the cells were centrifuged at 200 g and washed twice with PBS buffer. Next, 4×10^5 cells were resuspended in 200 µl of Annexin V binding buffer. From this suspension, 100 µl was transferred to a new microtube, and 10 µl of PI (100 $\mu g.ml^{-1}$) and 5 µl of Annexin V-FITC solution were added. This mixture was incubated for 15 min in the dark. Finally, 400 µl of binding buffer was added. The stained cells were then analyzed using flow cytometry (BD Biosciences, USA) to distinguish between viable ($Annexin\ V^-, PI^-$) and early apoptotic cells ($Annexin\ V^+, PI^-$), late apoptotic/necrotic cells ($Annexin\ V^+, PI^+$). The apoptosis assay was conducted in triplicate.

Results

Characterization of fabricated carrier

The XRD pattern depicted in Fig. 1. illustrates the diatomaceous silica powder within the 2-theta range of 0 to 80 degrees. This pattern confirms the amorphous structure of diatomaceous silica.

Transmission electron microscopy analysis was used to achieve the structure and morphology of the biosilica nanocarrier, and the images are presented in Fig. 2. The TEM images of the biosilica at 50, 100, and 200 nm scales reveal a porous and amorphous structure with irregularly distributed voids and a rough surface texture. The images highlight the presence of interconnected pores within the biosilica, which are consistent with the high surface area (15.16 $m^2.g^{-1}$) and pore size distribution (130–160 nm) observed in BET analysis. The amorphous

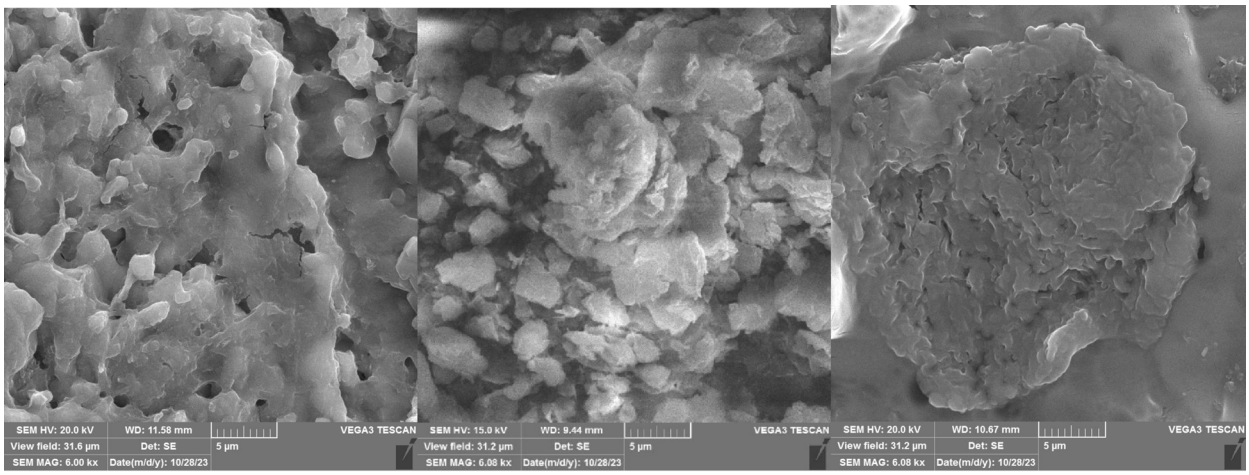

[A] [B] [C]

Fig. 3. Scanning electron microscopy images of (**A**) diatom, (**B**) diatom biosilica, and (**C**) DOX-loaded functionalized biosilica.

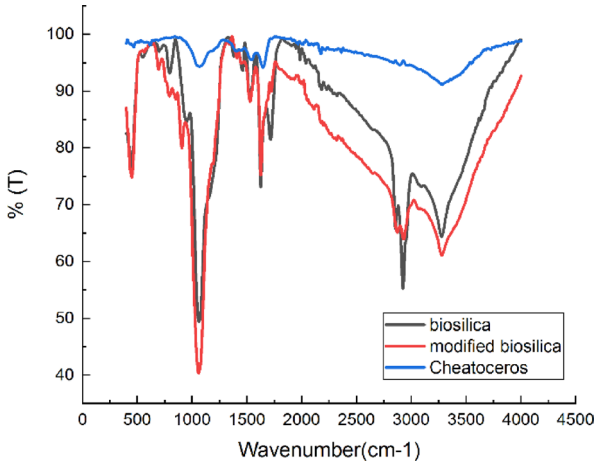

Fig. 4. Fourier Transform Infrared Spectroscopy of *Chaetoceros* sp., extracted biosilica, and modified biosilica.

nature of the material, as confirmed by XRD, is evident in the lack of crystalline patterns, while the structural integrity of the particles suggests mechanical stability suitable for drug loading and release applications.

Scanning electron microscopy (SEM) analysis showed the biosilica surface's microstructure and textural characteristics at submicrometer scales. The SEM images (Fig. 3) show the morphology of *Chaetoceros* sp. and the lateral view of diatom frustules at 2, 5, and 100 µm. The obtained images of biosilica confirmed the amorphous structure.

Fourier Transform Infrared Spectroscopy (FTIR) was employed to investigate variations in the surface chemistry of nanoparticles. The FTIR spectra of the *Chaetoceros* sp. frustules, before purification, the purified biosilica, and the functionalized frustules are shown in Fig. 4. The bands at 447, 794, and 1062 cm^{-1}, evident in the spectra, can be attributed to the asymmetric stretching or bending vibrations of Si–O-Si bonds. The valley at 3278 cm^{-1} in the spectrum of the silica frustule and the band at 3282 cm^{-1} in the diatom spectrum are associated with the bending vibrations of the OH groups of adsorbed water (corresponding to OH vibrations). These OH groups, along with the Si–OH stretching vibration observed at 950 cm^{-1} in the silica frustule spectrum and at 906 cm^{-1} in the modified silica spectrum, play a critical role in the adsorption of DOX (doxorubicin) via hydrogen bonding. The hydroxyl and amino groups of DOX interact with the silanol (Si–OH) groups on the biosilica surface, facilitating drug loading. The presence of GPTMS (3-glycidyloxypropyl trimethoxysilane) in the modified silica is indicated by the CH band at 2931 cm^{-1}, which is shifted compared to the bands at 2892 cm^{-1} in the Chaetoceros spectrum and 2925 cm^{-1} in the silica frustule spectrum. GPTMS introduces epoxy groups, which are essential for the covalent attachment of anti-CD19 antibodies. The epoxy groups react with the primary amine groups (-NH_2) of the antibodies, forming stable covalent bonds. This is supported by the

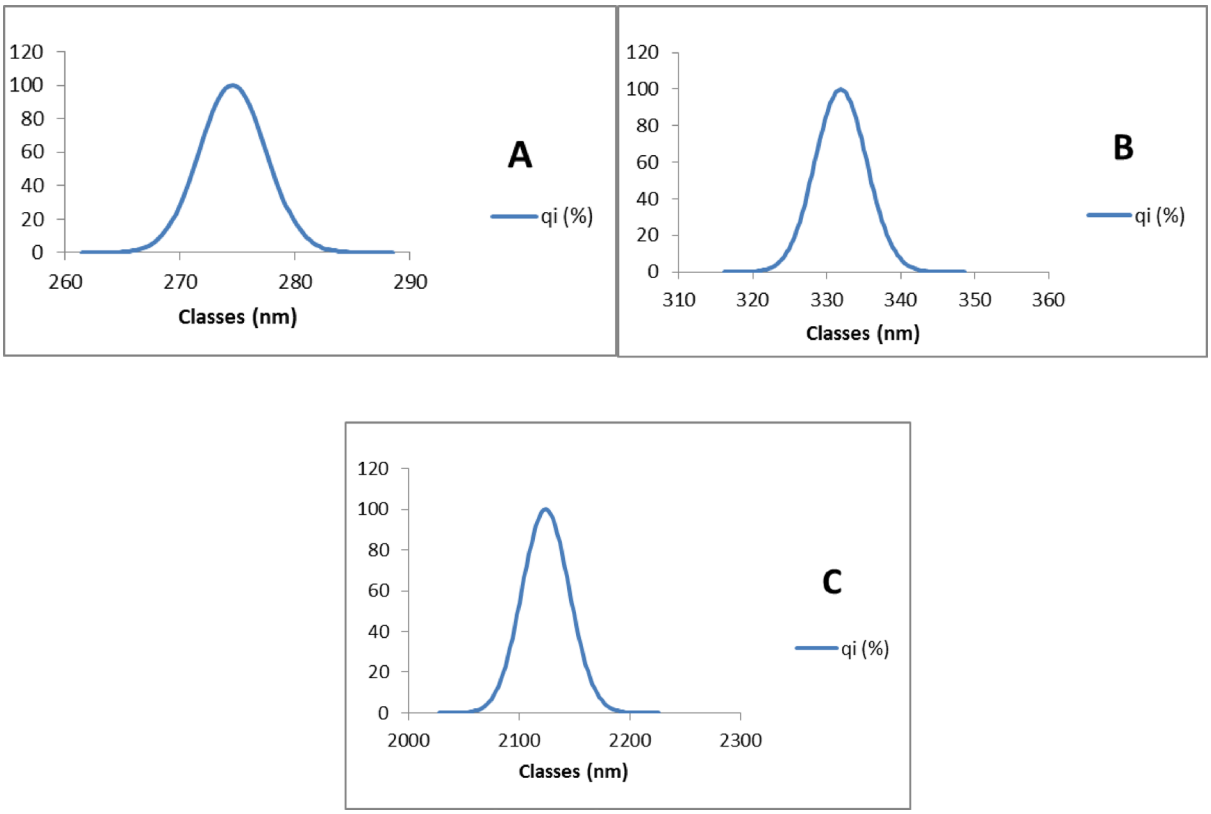

Fig. 5. DLS graphs (the x-axis represents diameter and the y-axis represents relative frequency) of *Cheatoceros* frustules (**A**), surface-modified biosilica (**B**), and DOX-loaded biosilica carrier (**C**).

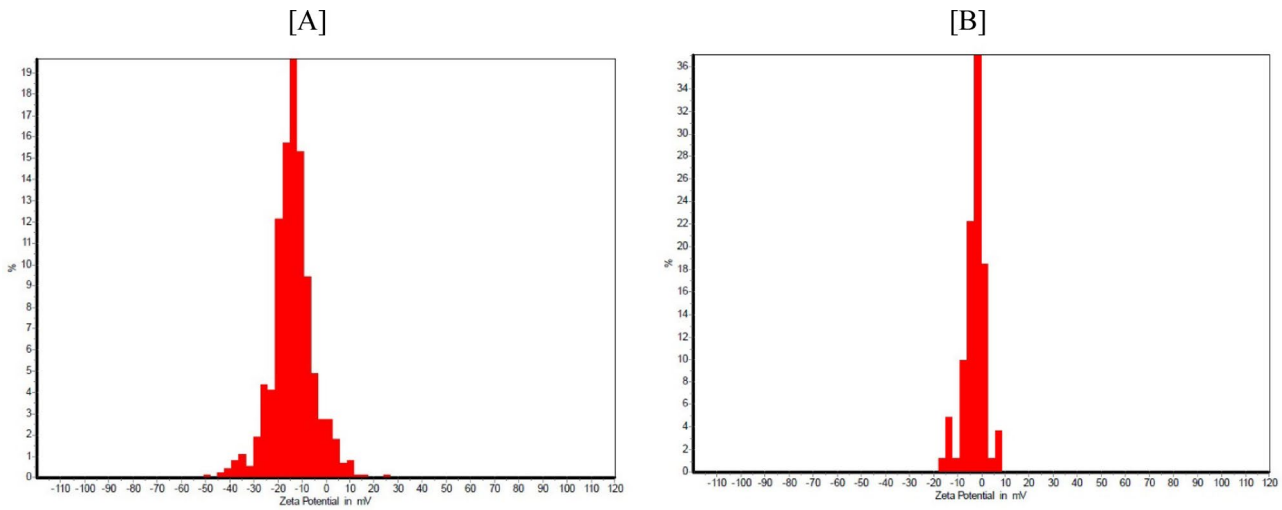

Fig. 6. Zeta potential of Cheatocerose biosilica (**A**) and functionalized drug-loaded biosilica (**B**).

presence of NH groups, as indicated by the bands at 1644 cm^{-1} in the diatom spectrum and 1627 cm^{-1} in both the silica frustule and modified silica spectra·

The histogram from dynamic light scattering analysis depicting the size distribution of silica frustules, modified silica, and drug-containing complexes is presented in Fig. 5, respectively. The peaks in the blue-colored graphs indicate the particle counts, which are reported to the highest particle counts at 275 nm, 333 nm, and 2.12 µm, respectively.

The surface potential of the unfunctionalized diatom frustules was measured at – 16 mV, as shown in Fig. 6. GPTMS-treated biosilica, however, showed a surface potential of – 13 mV. Following the conjugation of anti-CD19 monoclonal antibodies (mAbs) and loading of doxorubicin (DOX) the overall.

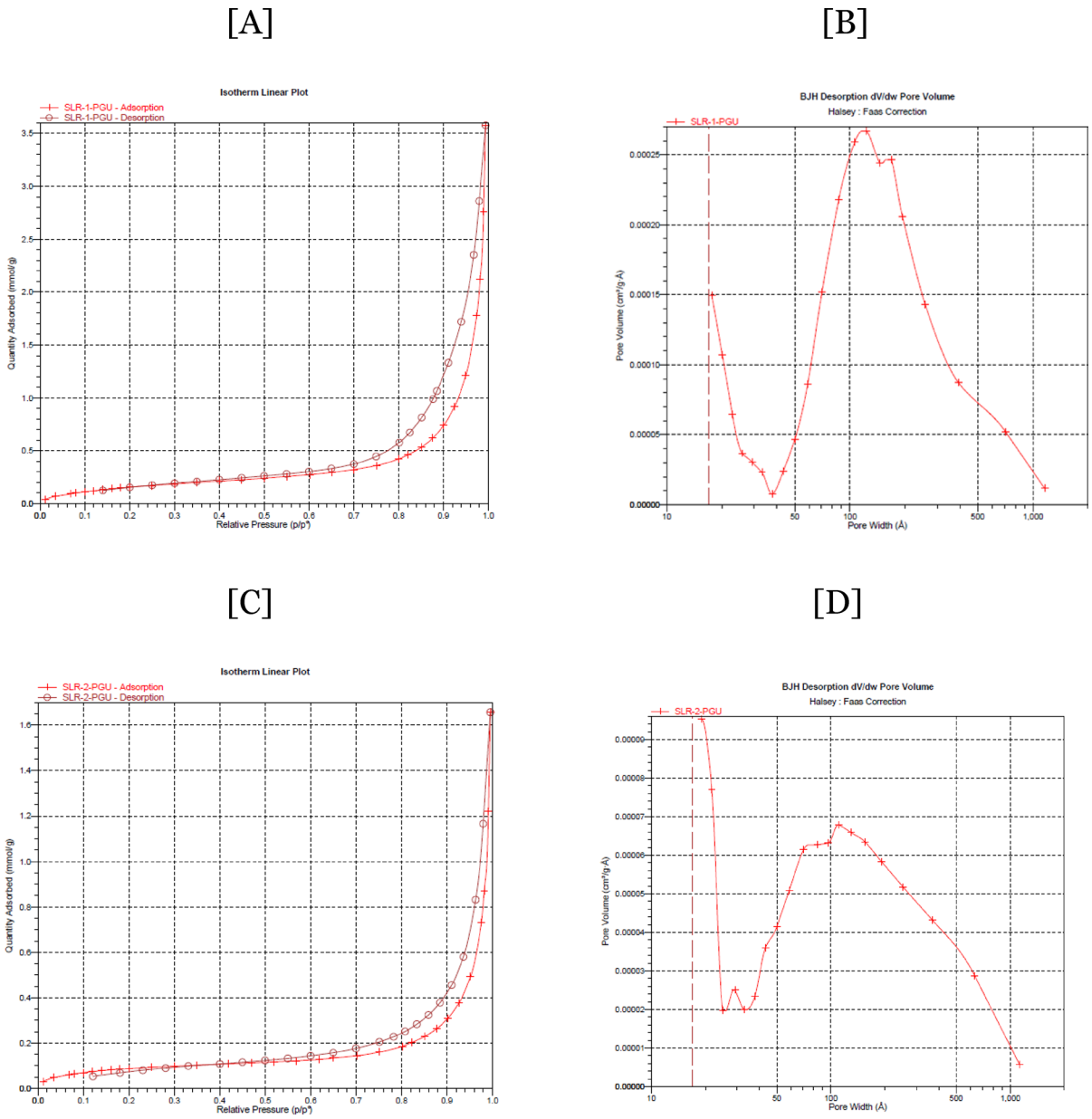

Fig. 7. The results of BET analysis show (**A**) absorption (+) desorption (∘) isotherms of cleaned frustule, (**B**) Diagram of the pore volume distribution of biosilica, (**C**) Absorption (+) desorption (∘) isotherms of modified Biosilica (**D**) Diagram of the pore volume distribution of biosilica after surface modification with GPTMS. *Note* Pore size distributions reflect intraparticle porosity measured by nitrogen adsorption.

	Specific surface area ($m^2\ g^{-1}$)	Total pore volume ($cm^3\ g^{-1}$)	Pore diameter (nm)
Biosilica	15.16	0.06	162.40
Functionalized biosilica	7.63	0.02	132.73

Table 1. Pore diameter, total pore volume, and specific surface area of Chaetoceros cleaned frustules and functionalized biosilica obtained from BET analysis.

surface potential further increased to − 2.74 mV.

The adsorption–desorption isotherms of N2, pore size distribution, and pore volumes of *Chaetoceros* sp. frustules and GPTMS-treated biosilica are presented in Fig. 7. The specific surface area, pore volume, and average pore diameter are summarized in Table 1. An analysis of the adsorption–desorption isotherms reveals typical type IV adsorption isotherms, characteristic of mesoporous materials, as well as H3-type hysteresis loops.

The onset of capillary condensation in the modified silica occurs at a lower pressure range compared to that of the frustule, indicating a systematic reduction in pore size. The pore diameters for frustule and modified silica are observed to be 160 nm and 130 nm, respectively. According to the results obtained, the pores observed in the biogenic silica of this study are envisioned as conical fractals.

Drug loading

Different concentrations of unloaded DOX were measured following six dilutions in the wavelength range of 320 to 740 nm to examine the extent of drug loading. As the graph in Fig. 8. indicates, this part of the study involved drug concentrations ranging from 0.00078 to 0.025 ml. Displacement advancements were observed at concentrations of 0.0125 and 0.00625.

For the calculation of drug loading capacity, 10 mg of diatom powder was incubated in 1 ml of a chemotherapy solution of doxorubicin at a concentration of 0.2 $mg.mL^{-1}$ for 24 h at room temperature with magnetic stirring. Subsequently, the mixture was centrifuged at 1400 rpm to separate the precipitate from the solution. The residual solution was measured for absorbance, and the drug loading efficiency of %53.92 was calculated.

Drug release

In order to study the performance of fabricated biosilica in drug delivery applications, in vitro drug release was studied at different time intervals for 48 h. The experiments were conducted at pH 5.0 and 7.5 to simulate the pH values of the tumor microenvironment and the physiological environment, respectively. It was revealed that doxorubicin release from the functionalized carrier was pH-dependent (Fig. 9). The rate of DOX release increased at the higher pH of 7.5. The functionalized biosilica reached a stable release after 35 h at both pH conditions, however, more intense drug release was observed at pH 5 compared to neutral pH.

Fluorescent microscopy imaging

Fluorescence imaging revealed the uptake of anti-CD19 MBS/DOX by Raji cells. Leveraging the intrinsic fluorescent properties of biosilica, the internalization of anti-CD19 MBS/DOX was analyzed in both Raji and Jurkat cells using fluorescence microscopy. As shown in Fig. 10, the green fluorescence, corresponding to an emission wavelength of 520 nm, was prominently observed in Raji cells, indicating a significantly higher uptake of anti-CD19 MBS/DOX. In contrast, only a small fraction of Jurkat cells exhibited detectable green fluorescence, with the intensity being markedly fainter compared to Raji cells. This difference in fluorescence intensity directly reflects the extent of anti-CD19 MBS/DOX internalization, confirming that Raji cells demonstrate substantially greater uptake than Jurkat cells.

Anti-CD19 MBS/DOX were more cytotoxic than MBS/DOX for Raji cells

In order to investigate the effects of anti-CD19 MBS/DOX on the viability of Raji and Jurkat cells, the MTT assay was employed using different concentrations of anti-CD19-MBS/DOX ranging from 0.1 to 1.6 $mg.mL^{-1}$ over 24 h. As illustrated in Fig. 11A, the drug-carrying biosilica complex resulted in significant cytotoxicity in a concentration-dependent manner in Raji and Jurkat cells as the relative OD absorbance decreased. Furthermore, the anti-CD19 MBS/DOX showed higher toxicity for Raji cells (CD19 +) than for Jurkat cells (CD19 +). Moreover, the IC_{50} of anti-CD19 MBS/DOX on Raji cells was calculated as 0.12 $mg.mL^{-1}$ at 24 h.

To evaluate the targeted effect of the anti-CD19 MBS/DOX, its impact at 0.12 $mg.mL^{-1}$ was assessed on Raji and Jurkat cells in comparison with MBS/DOX at similar concentration. As shown in Fig. 11B, the anti-CD19 MBS/DOX, demonstrated a more cytotoxic effect on Raji cells than MBS/DOX, while the effects of anti-CD19 MBS/DOX and MBS/DOX on Jurkat were comparable, indicating that anti-CD19 MBS/DOX has a more specific cytotoxicity on Raji cells.

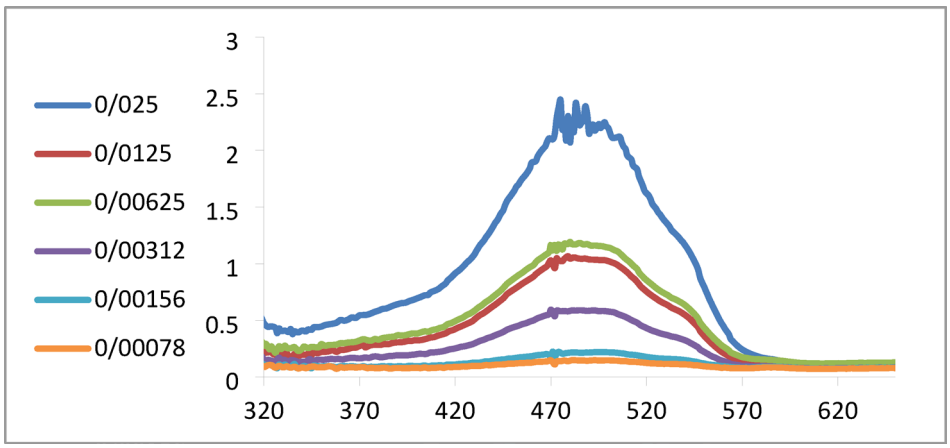

Fig. 8. Absorption of standard solutions of the drug doxorubicin.

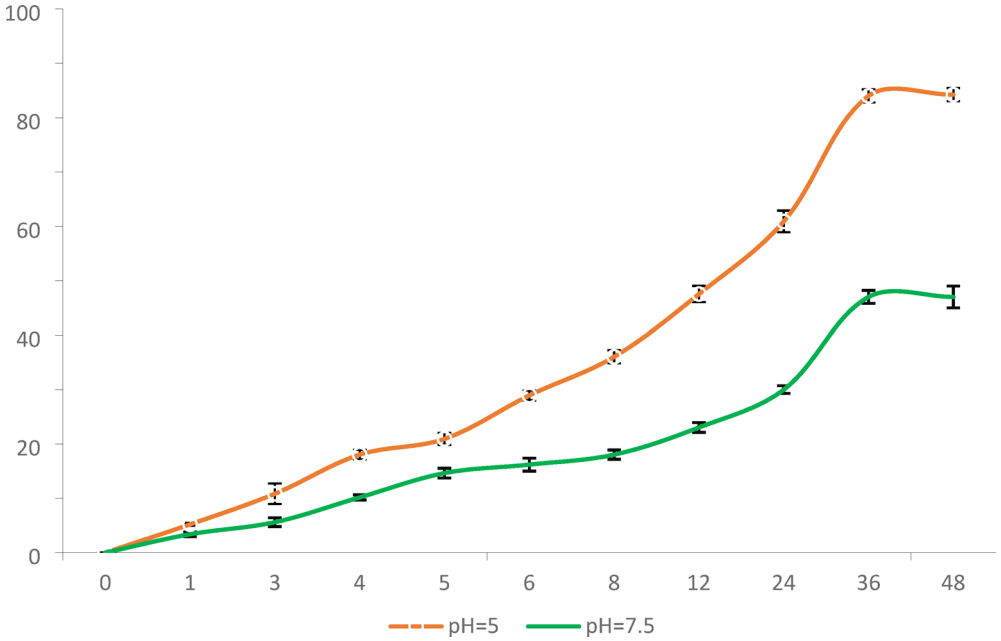

Fig. 9. The graph of Doxorubicin release from the modified biosilica carrier. Drug release was analyzed at pH 5.0 and 7.5 to simulate the pH values of the tumor microenvironment and the physiological environment, respectively.

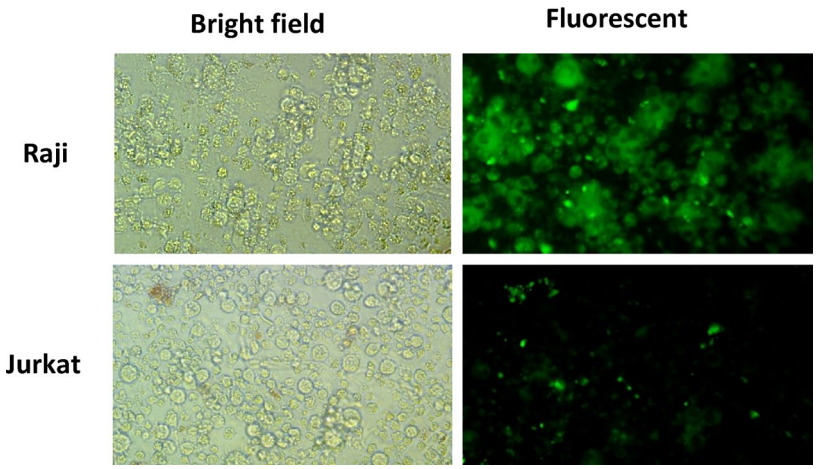

Fig. 10. The qualitative fluorescence microscopy bioimaging of cellular uptake of anti-CD19 MBS/DOX in Raji and Jurkat cells.

Anti-CD19 MBS/DOX, induced more apoptosis in Raji cells

To investigate the impact of anti-CD19 MBS/DOX on the death of Raji and Jurkat cells, flow cytometry analysis was performed 24 h after treatment using Annexin V-PI staining. Figure 12 demonstrate that anti-CD19 MBS/DOX induced apoptosis in both cell types; however, the percentage of apoptotic cells were higher among anti-CD19 MBS/DOX-treated Raji cells compared to Jurkat cells. Indeed, Fig. 12B illustrates that the mean percentage of apoptotic cells (early and late apoptosis) in untreated Jurkat cells was 0.33%, while it was 28.8% in anti-CD19 MBS/DOX-treated Jurkat cells. For Raji cells, the mean percentage of apoptotic cells was about 0.6% in untreated cells and 45.95% in cells treated with anti-CD19 MBS/DOX.

Discussion

Based on the data provided here, the concept of utilizing *Caetoceros* sp. biosilica is practical, as they concurrently can be antibody-labeled and loaded by DOX. The surface-functionalized, antibody-labeled, DOX-loaded biosilica significantly inhibited target cancer cell proliferation compared to non-target cells. This potential activity will significantly reduce the side effects of cancer medications in the body.

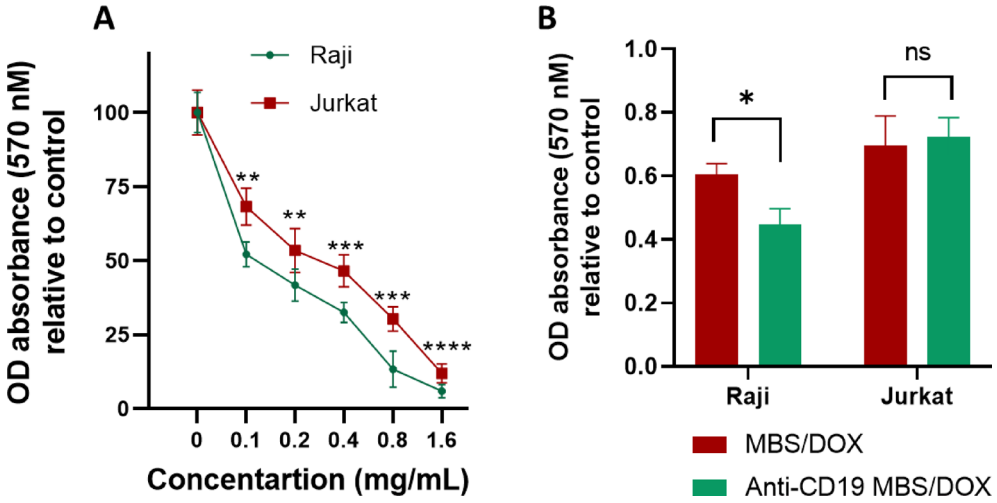

Fig. 11. Cell viability assessment via MTT assay was conducted over 24 h. (**A**) Following treatment with anti-CD19 MBS/DOX, cytotoxicity was assessed using the MTT assay at the 24-h time point, with OD absorbance at 570 nm presented as mean ± standard deviation relative to control. (**B**) The effect of anti-CD19 MBS/DOX and MBS/DOX on Raji and Jurkat cells. Cells were treated for 24 h with a concentration of 0.12 mg/mL of either anti-CD19 MBS/DOX or MBS/DOX, and cytotoxicity was assessed using the MTT assay. The relative OD absorbance at 570 nm is presented as mean ± standard deviation. Comparisons between the control group and various treatment groups were conducted using one-way ANOVA followed by Tukey's post-hoc test (* = $p < 0.05$, ** = $p < 0.01$, *** = $p < 0.001$, **** = $p < 0.0001$).

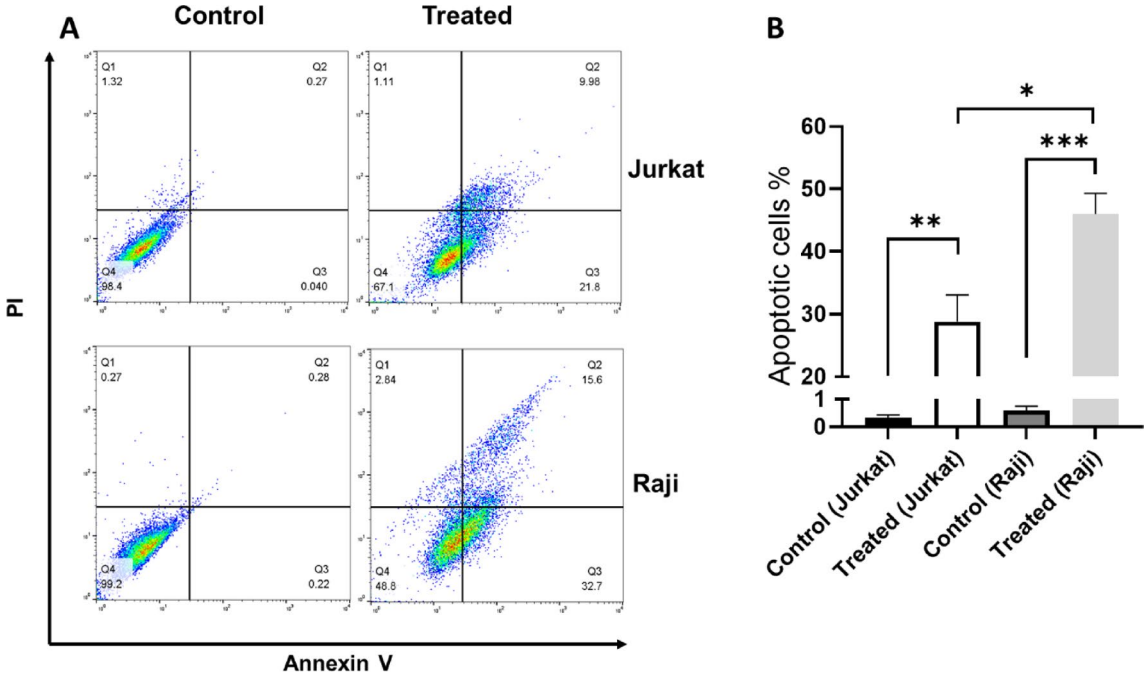

Fig. 12. The effect of anti-CD19 MBS/DOX on Jurkat and Raji cell apoptosis. (**A**) Flow cytometry analysis of anti-CD19 MBS/DOX-treated cells compared with untreated cells at 24 h. (**B**) The mean ± SD percentage of apoptotic cells among anti-CD19 MBS/DOX-treated cells and untreated cells (n = 3). SD = standard deviation, n = number of replicates, * = $p < 0.05$, ** = $p < 0.01$, *** = $p < 0.001$.**

Enhancing efficiency and specificity for cancer cells is essential to achieve the optimum effectiveness of a drug delivery platform. Intensive investigations have been performed to develop efficient drug carriers that are natural, biocompatible, and biodegradable, with the capability to identify unique cell-specific markers and bind to specific cancer cells. Porous biosilica particles meet all these criteria and are considered promising microscale

drug vehicle[14,22]. In addition, their efficiency in releasing hydrophobic drugs and extended-release profile, high surface area, as well as thermal and mechanical stability signify their importance[13,14,31,32].

The XRD pattern of biosilica was comparable to other studies on silica from biological sources. The diffused peak observed around 20 degrees corresponds to the characteristic peak (~ 20–26° two theta) associated with amorphous biosilica which is commonly called opal-A[33,34].

The zeta potential of biosilica increased following the functionalization process, and more elevation was observed after antibody labeling and DOX loading. It appears that the surface potential of GPTMS-treated biosilica slightly increased as a result of the reaction between the silane and water (dissolution) and subsequent detachment from the silica surface. This elevation of zeta potential following antibody and DOX loading indicates that the amino group of DOX is persistently exposed on the surface of the biosilica carrier. These findings confirm the successful formulation of the DOX/FBS-CD19 drug carrier.

A higher specific surface area value corresponds to an increased porosity of the material. Conversely, a smaller specific surface area value correlates with narrower pores. This is an important feature when a porous compound is used as a drug carrier. The size and distribution of pores correspond to the carrier's drug loading and release properties. Diatom biosilica, a naturally derived biogenic nanoporous SiO_2, features a significant surface area and a high concentration of silanol groups (Si–OH), which allow for covalent bonding with functional biomaterials to create controlled drug delivery systems, as well as the adsorption of therapeutic agents such as proteins or drug molecules. In the present study, *Chaetoceros* sp. biosilica showed a specific surface area of 15.16 $m^2.g^{-1}$. The surface area of diatom biosilica has been reported between 1.4 and 51 $m^2.g^{-1}$, however, the efficiency of drug loading and release is further affected by the pores' size and distribution[35,36].

The observed fractal dimension of BS has unique advantages in revealing discontinuities and irregularities of the pore structure and can describe the pores' morphological complexity and spatial distribution.

The results of the FTIR analysis were comparable to the previously reported modified silica, indicating the successful adjoining of the GPTMS onto the surface of diatom biosilica[37].

The results of BET analysis indicated the mesoporous characteristics. A higher specific surface area value corresponds to an increased porosity of the material. The pore diameters for frustule and modified silica exhibit maxima of 162.406 nm and 132.736 nm, respectively. The onset of the capillary condensation phase for modified biosilica occurs at a lower pressure range compared to frustule, which suggests a systematic reduction in pore size. Following surface modification, the pore diameter was reduced by approximately 19%. As noted by other researchers, the reduction in pore size can be attributed to the successful modification of the surface[38].

The large pore size enables the effective loading of macromolecules such as anticancer drugs. The fractal dimension indicates that the pore size distribution of silica-based materials varies at the microscale. Additionally, the specific surface area, which decreased from 15 to 7, suggests that the pores have been filled with functional groups, antibodies, and drugs, leading to a corresponding increase in size.

In the present study, doxorubicin, which is a highly hydrophobic chemotherapy agent used widely in clinical cancer treatments, was successfully loaded on fabricated modified biosilica. The efficient loading capacity of %53.92 can be attributed to porosity, surface charge, and surface modification with hydrophilic GPTMS[39,40]. The intrinsic nanostructure of diatoms biosilica play an important role in the loading capacity and extended release[41].

In this study, the anti-CD19 antibody was utilized to enhance the specificity of the MBS/DOX complex toward CD19 + Raji cells. The MTT assay confirmed that the anti-CD19 MBS/DOX complex had a more cytotoxic effect on Raji cells compared to Jurkat cells, in contrast to MBS/DOX alone. Additionally, apoptosis analysis by flow cytometry demonstrated the specificity of the anti-CD19 MBS/DOX complex for Raji cells, as a higher percentage of apoptotic cells was observed among anti-CD19 MBS/DOX-treated Raji cells compared to Jurkat cells. Previous studies have supported the use of Raji cells as target cells and Jurkat cells as non-target cells in lymphoma-targeted delivery research[42]. Furthermore, our strategy to enhance specific cell cytotoxicity and apoptosis, supported by MTT and apoptosis assays, aligns with the findings of Xu et al. They demonstrated that anti-CD22-conjugated cadmium-tellurium quantum dots co-loaded with doxorubicin (DOX) and gambogic acid exhibited a more targeted effect on cell cytotoxicity and apoptosis in Raji cells ($CD22^+$) compared to Jurkat cells ($CD22^-$)[42].

Although no study has utilized the anti-CD19 antibody to improve the specificity of Chaetoceros mesoporous silica against lymphoma cells, the potential of using antibodies to enhance the specificity of diatoms has been previously reported. For instance, Esfandyari et al. demonstrated the attachment of trastuzumab to diatoms to specifically capture HER2-positive cells[14]. The study demonstrates that biosilica derived from *Chaetoceros* sp. exhibits a drug loading capacity of 53.92% and pH-dependent release, with significant cytotoxicity and apoptosis induction in Raji cells (IC50 = 0.12 $mg.mL^{-1}$). While chemically synthesized silica often shows higher stability and controlled pore sizes, biosilica offers unique advantages such as natural origin, biocompatibility, and eco-friendliness, aligning with green chemistry principles. For instance, chemically synthesized silica typically achieves higher surface areas (e.g., 100–1000 $m^2.g^{-1}$)[43] compared to biosilica (15.16 $m^2.g^{-1}$ in this study), which may enhance drug loading efficiency. However, biosilica's intrinsic nanostructure and biodegradability make it a promising alternative for sustainable drug delivery, despite the need for further optimization to match the stability and efficacy of synthetic counterparts[18]. Future research should focus on addressing these limitations to bridge the gap between natural and chemically synthesized silica for clinical applications.

The study highlights the potential of functionalized *Chaetoceros* mesoporous silica as a targeted drug delivery system for B-cell lymphoma, demonstrating effective doxorubicin loading, pH-dependent release, and enhanced cytotoxicity and apoptosis in Raji cells compared to non-target Jurkat cells. However, further research is needed to ensure the system's biocompatibility and bioaccumulation safety, as the current formulation requires optimization for in vivo applications. Future studies should focus on in vivo testing, combination therapies,

scalability, and advanced characterization to address these limitations and explore broader applications in cancer treatment and other diseases.

Conclusion

The purification of diatomaceous frustule from *Chaetoceros* sp. resulted in the formation of biosilica with an amorphous structure. The successful modification of the diatom surface with GPTMS functional groups was clearly demonstrated. The loading capacity and drug release properties of the diatom microparticles were successfully altered under laboratory conditions by functionalizing the diatom surfaces with organic sections containing various hydrophobic and hydrophilic groups for the model drug.

The modified porous structure successfully conjugated with anti-CD19, creating a structure capable of loading doxorubicin. Cellular assays demonstrated that this drug delivery system effectively facilitated drug transportation to targeted RAJI cells, resulting in greater cytotoxicity compared to non-target Jurkat cells, which underscores its therapeutic potential. It is recommended that the application of this approach be explored in clinical and laboratory studies involving other drugs in conjunction with various combination therapies for enhanced efficacy.

Data availability

The authors declare that the data underpinning the results of this study can be found in the main text and the Supplementary Information files. If any raw data in a different format is required, it can be obtained by contacting the corresponding author.

Received: 12 January 2025; Accepted: 6 May 2025
Published online: 13 May 2025

References

1. Chu, Y. et al. The epidemiological patterns of non-Hodgkin lymphoma: global estimates of disease burden, risk factors, and temporal trends. *Front. Oncol.* **13**, 1059914 (2023).
2. Jamil, A. & Mukkamalla, S. K. R. Lymphoma. In: StatPearls. Treasure Island (FL): StatPearls Publishing; 2023 [cited 2023 Nov 5]. Available from: http://www.ncbi.nlm.nih.gov/books/NBK560826/
3. Wang, M. Y. et al. Methotrexate-loaded biodegradable polymeric micelles for lymphoma therapy. *Int J Pharm.* **557**, 74–85 (2019).
4. Xu, P. et al. Doxorubicin-loaded platelets as a smart drug delivery system: An improved therapy for lymphoma. *Sci. Rep.* **7**(1), 42632 (2017).
5. Sapkota, S. & Shaikh, H. Non-hodgkin lymphoma. In: StatPearls [Internet]. Treasure Island (FL): StatPearls Publishing; 2023 [cited 2023 Nov 5]. Available from: http://www.ncbi.nlm.nih.gov/books/NBK559328/
6. Patel, U., Rathnayake, K., Singh, N. & Hunt, E. C. Dual targeted delivery of liposomal hybrid gold nano-assembly for enhanced photothermal therapy against lung carcinomas. *ACS Appl. Biol. Mater.* **6**(5), 1915–1933 (2023).
7. Kyriazi, M. E. et al. Multiplexed mRNA sensing and combinatorial-targeted drug delivery using DNA-gold nanoparticle dimers. *ACS Nano* **12**(4), 3333–3340 (2018).
8. Sarkis, M. et al. D2B-functionalized gold nanoparticles: promising vehicles for targeted drug delivery to prostate cancer. *ACS Appl. Biol. Mater.* **6**(2), 819–827 (2023).
9. Arora, V., Abourehab, M. A., Modi, G. & Kesharwani, P. Dendrimers as prospective nanocarrier for targeted delivery against lung cancer. *Eur. Polym. J.* **180**, 111635 (2022).
10. Doppalapudi, S., Jain, A., Domb, A. J. & Khan, W. Biodegradable polymers for targeted delivery of anti-cancer drugs. *Expert Opin. Drug. Deliv.* **13**(6), 891–909 (2016).
11. Fu, C. P. et al. Hyaluronic acid-based nanocarriers for anticancer drug delivery. *Polymers* **15**(10), 2317 (2023).
12. Iranshahy, M. et al. Curcumin-loaded mesoporous silica nanoparticles for drug delivery: synthesis, biological assays and therapeutic potential–a review. *RSC Adv.* **13**(32), 22250–22267 (2023).
13. Fang, L. et al. The application of mesoporous silica nanoparticles as a drug delivery vehicle in oral disease treatment. *Front. Cell Infect. Microbiol.* **13**, 1124411 (2023).
14. Esfandyari, J. et al. Capture and detection of rare cancer cells in blood by intrinsic fluorescence of a novel functionalized diatom. *Photodiagn. Photodyn. Ther.* **30**, 101753 (2020).
15. Uthappa, U. T. et al. Nature engineered diatom biosilica as drug delivery systems. *J. Controlled Release.* **1**, 281 (2018).
16. Vona, D. et al. Drug delivery through epidermal tissue cells by functionalized biosilica from diatom microalgae. *Mar. Drugs* **21**(8), 438 (2023).
17. Peng, G. et al. Facile fabrication of diatomite biosilica-based nasal drug delivery vehicle for enhanced treatment of allergic rhinitis. *Colloids Surf. B Biointerfaces* **234**, 113715 (2024).
18. Losic, D. et al. Surface functionalisation of diatoms with dopamine modified iron-oxide nanoparticles: Toward magnetically guided drug microcarriers with biologically derived morphologies. *Chem. Commun.* **46**(34), 6323 (2010).
19. Sasirekha, R. & Santhanam, P. Surface bioengineering of diatom by amine and phosphate groups for efficient drug delivery. *Basic Appl. Phytoplankton Biol.* 229–237 (2019).
20. Youn, S., Ki, M. R., Min, K. H., Abdelhamid, M. A. A. & Pack, S. P. Antimicrobial and hemostatic diatom biosilica composite sponge. *Antibiotics* **13**(8), 714 (2024).
21. Bai, J. W., Qiu, S. Q. & Zhang, G. J. Molecular and functional imaging in cancer-targeted therapy: Current applications and future directions. *Signal Transduct Target Ther.* **8**(1), 1–32 (2023).
22. Liu, B., Zhou, H., Tan, L., Siu, K. T. H. & Guan, X. Y. Exploring treatment options in cancer: tumor treatment strategies. *Signal Transduct Target Ther* **9**(1), 1–44 (2024).
23. Tiwari, H. et al. Recent advances in nanomaterials-based targeted drug delivery for preclinical cancer diagnosis and therapeutics. *Bioengineering* **10**(7), 760 (2023).
24. Cave, D. D., Mangini, M., Tramontano, C., Stefano, L. D., Corona, M. & Rea, I., et al. Hybrid biosilica nanoparticles for in-vivo targeted inhibition of colorectal cancer growth and label-free imaging. *Int. J. Nanomed* (2024). https://doi.org/10.2147/IJN.S480168
25. Wang, K., Wei, G. & Liu, D. CD19: A biomarker for B cell development, lymphoma diagnosis and therapy. *Exp. Hematol. Oncol.* **1**(1), 36. https://doi.org/10.1186/2162-3619-1-36 (2012).
26. Pan, H., Li, S., Li, M., Tao, Q., Jia, J., & Li, W., et al. Anti-CD19 mAb-conjugated human serum albumin nanoparticles effectively deliver doxorubicin to B-lymphoblastic leukemia cells (2020).

27. Brudno, J. N., Lam, N., Vanasse, D., Shen, Y., Rose, J. J.& Rossi, J., et al. Safety and feasibility of anti-CD19 CAR T cells with fully human binding domains in patients with B-cell lymphoma. *Nat. Med.* **26**(2), 270–280 (2020).
28. Li, X., Wang, X., Qian, G. & Ito, A. Synergistical chemotherapy and cancer immunotherapy using dual drug-delivering and immunopotentiating mesoporous silica. *Appl. Mater. Today* **16**, 102–111 (2019).
29. Wang, X., Oyane, A., Inose, T. & Nakamura, M. In situ synthesis of a tumor-microenvironment-responsive chemotherapy drug. *Pharmaceutics* **15**(4), 1316 (2023).
30. Moorthy, M. S., Bharathiraja, S., Manivasagan, P., Lee, K. D. & Oh, J. Synthesis of surface capped mesoporous silica nanoparticles for pH-stimuli responsive drug delivery applications. *MedChemComm* **8**(9), 1797–1805 (2017).
31. Delalat, B. et al. Targeted drug delivery using genetically engineered diatom biosilica. *Nat. Commun.* **6**(1), 8791 (2015).
32. Su, C. et al. The hierarchical porous structures of diatom biosilica-based hemostat: From selective adsorption to rapid hemostasis. *J. Colloid Interface Sci.* **651**, 544–557 (2023).
33. Pannico, M. et al. Electroless gold-modified diatoms as surface-enhanced raman scattering supports. *Nanoscale Res. Lett.* **11**(1), 315. https://doi.org/10.1186/s11671-016-1539-x (2016).
34. Sprynskyy, M. et al. Naturally organic functionalized 3D biosilica from diatom microalgae. *Mater. Des.* **132**, 22–29 (2017).
35. Hussein, H. A., Nazir, M. S., Azra, N., Qamar, Z., Seeni, A. & Tengku Din, T. A., et al. Novel drug and gene delivery system and imaging agent based on marine diatom biosilica nanoparticles. *Mar Drugs* **20**(8), 480 (2022).
36. Vasani, R. B., Losic, D., Cavallaro, A. & Voelcker, N. H. Fabrication of stimulus-responsive diatom biosilica microcapsules for antibiotic drug delivery. *J. Mater. Chem. B* **3**(21), 4325–4329 (2015).
37. Pattanayek, S. & Ghosh, A. Dynamic shear rheology of colloidal suspensions of surface modified silica nanoparticles in PEG. *J. Nanopart. Res.* **24**, 20 (2018).
38. Li, K. M., Jiang, J. G., Tian, S. C., Chen, X. J. & Yan, F. Influence of silica types on synthesis and performance of amine-silica hybrid materials used for CO_2 capture. *J. Phys. Chem. C* **118**(5), 2454–2462. https://doi.org/10.1021/jp408354r (2014).
39. Kang, S. et al. A descriptive review on the potential use of diatom biosilica as a powerful functional biomaterial: A natural drug delivery system. *Pharmaceutics* **16**(9), 1171 (2024).
40. Maher, S. et al. From the mine to cancer therapy: Natural and biodegradable theranostic silicon nanocarriers from diatoms for sustained delivery of chemotherapeutics. *Adv. Healthc. Mater.* **5**(20), 2667–2678. https://doi.org/10.1002/adhm.201600688 (2016).
41. Lim, H. et al. Recent progress in diatom biosilica: A natural nanoporous silica material as sustained release carrier. *Pharmaceutics* **15**(10), 2434 (2023).
42. Xu, P. et al. Anti-CD22-conjugated CdTe QDs co-loaded with doxorubicin and gambogic acid: a novel platform for lymphoma treatment. *RSC Adv.* **7**(54), 33905–33913 (2017).
43. Slowing, I. I., Vivero-Escoto, J. L., Wu, C. W. & Lin, V. S. Y. Mesoporous silica nanoparticles as controlled release drug delivery and gene transfection carriers. *Adv. Drug Deliv. Rev.* **60**(11), 1278–1288 (2008).

Acknowledgements

The authors would like to thank Dr. Mohsen Mehrabi, Dr. Sadegh Karimi, and Mohammad Mozafarinia for their valuable advice and assistance throughout this project.

Author contributions

A.S. and A.A. wrote the main manuscript. G.S. and A.A. performed cell culture laboratory experiments. A.S. designed and conceptualized the project, and prepared figures and tables. H.N. and A.S. conducted the methodology of characterization techniques. G.S. and J.E. performed the microalgal culture and prepared and functionalized biosilica. G.S. conducted drug loading and release experiments and analysis. All authors reviewed the manuscript.

Declarations

Competing interests

The authors declare no competing interests.

Ethical approval

This study was conducted in accordance with the ethical principles outlined in the Declaration of Helsinki. This project was conducted under the supervision and approval of the Ethics Committee at the Persian Gulf University of Bushehr. The experimental protocols used in this study were designed and conducted to adhere to standard safety and ethical guidelines for cell culture and handling of biological materials.

Additional information

Correspondence and requests for materials should be addressed to A.S.